Industrial Chemistry & Materials

ROYAL SOCIETY OF CHEMISTRY

PAPER

View Article Online
View Journal | View Issue

Cite this: *Ind. Chem. Mater.*, 2024, **2**, 309

Ultrasonic assisted natural deep eutectic solvents as a green and efficient approach for extraction of hydroxytyrosol from olive leaves†

Mingming Hu,‡[ab] Bao Han,‡[c] Lin Xie,[ab] Beibei Lu,*[ab] De Bai,[ab] Nuo Shi,[d] Ya Liao,[c] Yan Wang,[c] Ling Liu,[c] Shaojun Wu,[c] Runrui Lan,[c] Xiaomei Lei,[c] Ci Shi,[c] Danhua Huang,[c] Yuanbin Li,[ab] Lin Lin*[d] and Jiaheng Zhang *[ab]

In this study, an ultrasonic assisted natural deep eutectic solvent (DES) was used to extract hydroxytyrosol (HT) from olive leaves. The optimal extraction conditions of the MaPa-4 concentration, extraction time and solid–liquid ratio were obtained by single factor experiments. The formation mechanism of MaPa and its interaction with HT were analyzed by FTIR, ^{1}H-NMR and density functional theory (DFT) calculation. Then, MaPa-4 and water extracts obtained under the optimal extraction conditions were selected for a series of efficacy tests. MaPa-4 extract demonstrated low cytotoxicity, good biocompatibility, and excellent anti-inflammatory and bacteriostatic properties. Overall, MaPa-4, as an environmentally friendly and efficient solvent, was combined with ultrasound treatment to develop an efficient, green and feasible method to extract HT from olive leaves.

Keywords: Hydroxytyrosol; Deep eutectic solvent; Single-factor experiment; Bacteriostatic; Anti-inflammatory; Antioxidant.

Received 20th May 2023,
Accepted 18th August 2023

DOI: 10.1039/d3im00055a

rsc.li/icm

1 Introduction

Olive is a woody oil tree of the genus *Olea* of the Oleaceae family, which has a cultivation history of more than 4000 years. It is native to Asia Minor, and is now mainly found in Italy, Spain, Greece, and other countries along the Mediterranean Sea.[1] China officially introduced olive in 1964, and the current cultivation areas include Gansu Longnan, Sichuan, *etc.*[2]

Olive leaves are rich in hydroxytyrosol (HT), oleuropein, vanillic acid,[3] luteolin,[4] caffeic acid, rutin and other active ingredients. The significant biological activity of olive leaves is mainly attributed to olpicrin[5,6] and its derivatives (HT and tyrosol). As an active substance with three hydroxyl groups,[7] HT is one of the most potent antioxidants, and its antioxidant capacity is ten times that of epicatechin and twice that of coenzyme Q10.[8] In addition, HT, as a functional food ingredient, also has excellent anti-inflammatory properties,[9–11] showing potential applications in treating diabetes,[12,13] arthritis,[14] liver damage[15] and cancer.[16,17]

Water and organic solvents (methanol and ethanol) have been used to extract phenolic compounds from olive leaves. Although the process of water extraction is simple, the extraction efficiency is unsatisfactory, and the polyphenols tend to decompose.[18,19] Traditional organic solvents are flammable and toxic, and the extraction involves high recovery cost and subsequent separation.[20] Therefore, it is urgent to develop efficient and green extraction solvents.

Deep eutectic solvents (DESs) are green and sustainable solvents[21,22] and are usually formed by combining two or three types of hydrogen bond acceptors (HBAs) and hydrogen bond donors (HBDs) through the interaction of hydrogen bonds.[23] As the research deepens, DESs find increasing applications in extraction of plant active substances, such as polyphenols,[24–26] phytosterols,[27] antibiotics,[28] germ proteins,[29] polysaccharides,[30] and flavonoids.[31,32] In addition to solvents, extraction methods are also important to achieve high extraction efficiency of active substances.[33] The ultrasonic assisted extraction method based on DESs has

[a] *Sauvage Laboratory for Smart Materials, Harbin Institute of Technology (Shenzhen), Shenzhen 518055, P. R. China. E-mail: lubeibei123123@163.com, zhangjiaheng@hit.edu.cn*
[b] *Research Centre of Printed Flexible Electronics, School of Materials Science and Engineering, Harbin Institute of Technology (Shenzhen), Shenzhen 518055, P. R. China*
[c] *Shenzhen Shinehigh Innovation Technology Co., Ltd, Shenzhen 518055, P. R. China*
[d] *Shanghai Corday Biotech. Co., Ltd, Shanghai 200000, P. R. China. E-mail: lin.lin@petersonslab.com*

† Electronic supplementary information (ESI) available: ESP analysis of each atom of matrine and panthenol. See DOI: https://doi.org/10.1039/d3im00055a

‡ Mingming Hu and Bao Han contributed equally to this work.

significant advantages, such as low cost, environmental friendliness, and high efficiency.[34,35]

Matrine is a natural alkaloid derived from the fruits, roots and plants of *Sophora flavescens* and has antiviral, anti-inflammatory and anti-bacterial effects.[36] Panthenol is a widely used vitamin B nutritional supplement, which protects the skin and mucous membranes with excellent moisturizing effect.[37] In this study, a series of matrine–panthenol (MaPa) DESs with different molar ratios were designed and prepared by combining density functional theory (DFT) calculation with experiments. MaPa DESs were used to extract HT from olive leaves with the assistance of ultrasound without the need for an additional separation process. Single factor experiments were performed to optimize the extraction conditions.[34,35] The mechanism of MaPa formation and ultrasound assisted extraction of HT was studied. A series of efficacy tests were conducted to compare the extract obtained under the optimal extraction conditions with the water extract. The extract obtained by this method is transparent, uniform and stable, which can be added as a raw material to

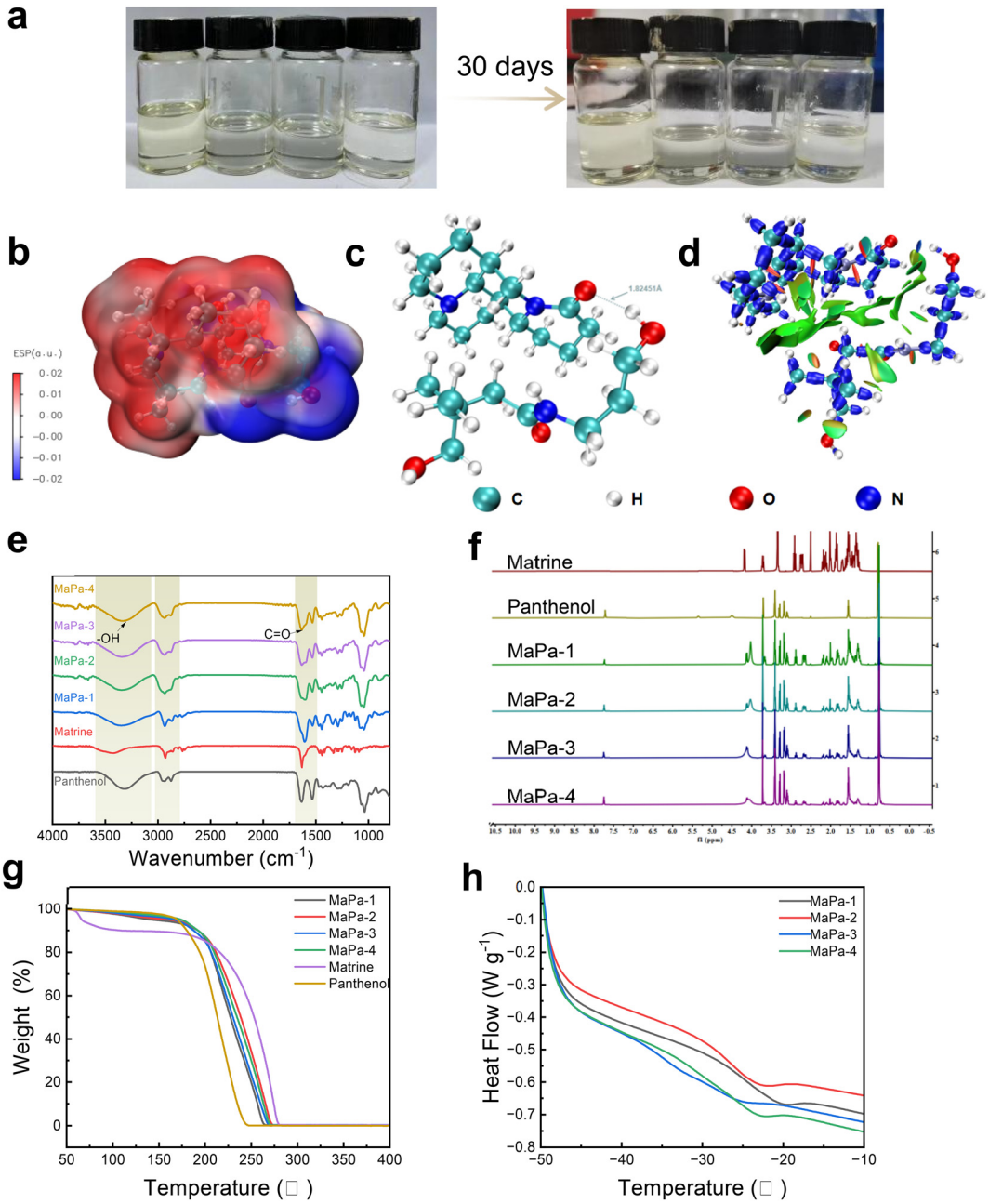

Fig. 1 Synthesis and characterization of DESs (MaPa). (a) Photos of MaPa: as prepared and after storage for one month; (b) ESP diagram (red: positively charged and blue: negatively charged); (c) structural optimization diagram; (d) IRI diagram (red: unbound overlaps; blue: strong attractive interactions; transition zone: van der Waals interactions); (e) FTIR spectra of various MaPa DESs; (f) ^{1}H NMR spectra of various MaPa DESs; (g) TGA and (h) DSC curves of MaPa DESs obtained with different molar ratios.

prepare skincare products for anti-inflammatory, antibacterial, and antioxidant purposes. This work provides a practical and theoretical basis for the application of olive extract in skincare products.

2 Results and discussion

2.1 Synthesis, optimization, and characterization of DESs

Four kinds of MaPa with different molar ratios were obtained at room temperature by heating and stirring. According to Fig. 1a, the color of the prepared MaPa did not change significantly after 30 days at room temperature, indicating that MaPa had good stability. Firstly, DFT calculation was used to predict the structure and the corresponding stability. According to ESP analysis (Fig. S1†), the amide region of matrine was negatively charged, while the corresponding panthenol hydroxyl region was positively charged. The positively charged region of panthenol was attracted to the negatively charged region of matrine, and the negatively charged region of panthenol was adjacent to the positively charged region of matrine, thus eventually forming a stable structure (Fig. 1c). As shown in Table S1,† the H17 of panthenol was the most electropositive, and the O1 on the amide group of matrine was the most electronegative, and they attracted each other to form a stable structure (Fig. 1b). The amide group of matrine and the hydroxyl group of panthenol had an interaction stronger than van der Waals force. In addition, van der Waals forces, hydrogen bonds and space repulsive forces were characterized by IRI analysis (Fig. 1d). A large transitional region existed between matrine and panthenol. The presence of blue discs between the amide group of matrine and the hydroxyl group of panthenol indicated strong hydrogen bonding forces at these sites. Structural optimization, ESP and IRI results all confirmed that the strong interaction between the two monomers contributed to the formation of MaPa.

Subsequently, the structure of MaPa was analyzed by FTIR and NMR. As shown in Fig. 1e, panthenol had a strong absorption peak from 3050 cm^{-1} to 3500 cm^{-1}, corresponding to the hydroxyl group. Panthenol and matrine had a sharp absorption peak from 1591 cm^{-1} to 1715 cm^{-1}, related to the carbonyl group. The peaks of MaPa from 3050 cm^{-1} to 3500 cm^{-1} and from 1591 cm^{-1} to 1715 cm^{-1} became broader with the increase in molar ratio, suggesting that the hydroxyl group of panthenol formed a hydrogen bond with the amide group of matrine. ^1H NMR analysis (Fig. 1f) showed a new proton peak at 4.10 ppm after the formation of the DES, while the matrine peak shifted to 3.46 ppm, and the H17 proton peak of panthenol at 4.39 ppm disappeared. The variations of the proton signals were attributed to the hydrogen bond or van der Waals interaction between matrine and panthenol, which agreed with the theoretical analysis. The results of DFT, FTIR and ^1H NMR confirmed the successful synthesis of the DES.

Finally, TGA and DSC were used to analyze the thermal stability of MaPa. TGA analysis showed that the decomposition temperature of MaPa was between 180 °C and 210 °C (Fig. 1g), suggesting the good thermal stability of MaPa. DSC analysis showed that the glass transition temperature was between −15 °C and 35 °C (Fig. 1h).

2.2 Influence of the solvent on extraction efficiency

The extraction rates of different solvents (water, methanol, and ethanol) and MaPa were compared, as shown in Fig. 2a. The extraction rates of MaPa with different molar ratios were better than those of the three control solvents. When the molar ratio of matrine to panthenol was 1 : 4, the extraction efficiency was the highest (1.63 times higher than that of water, 1.43 times higher than that of methanol and 2.07 times higher than that of ethanol). Through structural optimization (Fig. 2b), MaPa and HT had a stronger interaction than the van der Waals force and formed a stable structure. ESP analysis (Fig. 2c) confirmed the positive and negative potential attraction regions between MaPa and HT, and IRI analysis (Fig. 2d) showed large van der Waals weak interaction transition regions between MaPa and HT. Therefore, the high MaPa yield could be explained by the structural optimization, ESP and IRI results. For MaPa-4, a high panthenol ratio increased the number of molecules that could interact between MaPa and HT, leading to a high extraction efficiency.[35] Here, MaPa also acted as a green solvent, reducing waste and cost, and eliminating subsequent processing.

The olive leaves treated with different solvents were dried for SEM observation. As shown in Fig. 2e–j, the raw material of olive leaves without extraction had a large number of cracks and voids, and the surface was rough. Due to the cavitation effect of ultrasonic waves, a strong shear force is generated, which damages the microstructure of olive leaves and promotes the dissolution of active substances. The olive leaf powder treated with water, ethanol and methanol had some changes in the physical structure, and the surface became smooth, but a few rough particles were still exposed. After the extraction using MaPa-4, the surface tissue of olive leaves was obviously destroyed, forming smooth pieces. This indicated that the MaPa-4 extraction process could effectively damage the morphology of olive leaves, destroy cell walls, promote the dissolution of intracellular active components, and achieve higher extraction efficiency.

2.3 Single factor experiments

Single factor experiments were conducted to evaluate the influence of the MaPa-4 concentration, extraction time, and solid–liquid ratio on the extraction of HT. One parameter was varied when the other two parameters were fixed.

The effect of the MaPa-4 concentration on the HT yield was studied by using 10–90 wt% MaPa-4 (solid–liquid ratio: 40 mg mL^{-1} and extraction time: 60 min). With the MaPa-4 concentration increasing from 10 wt% to 60 wt%, the yield of HT increased significantly from 1.1 mg g^{-1} to 4.36 mg g^{-1} (Fig. 3a). When the concentration of MaPa-4 was more than 80 wt%, the extraction efficiency decreased significantly. As the concentration of MaPa-4 increased, more MaPa molecules

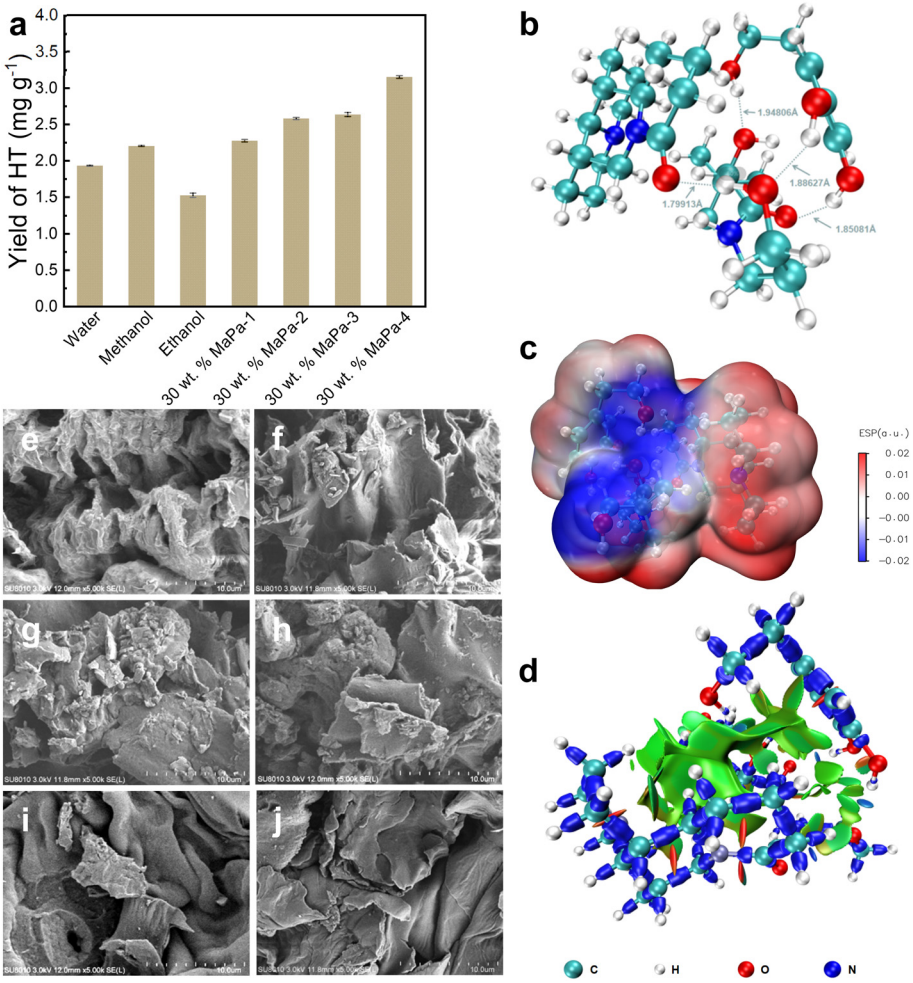

Fig. 2 (a) Yield of HT treated with different solvents; (b) structural optimization diagram of MaPa and HT; (c) ESP map of MaPa and HT; (d) IRI diagram of MaPa and HT; SEM images of olive leaves: (e) no treatment and treated with (f) water, (g) methanol, (h) ethanol, and (i and j) 30 wt% MaPa-4.

could interact with HT, enhancing the yield. However, when the MaPa-4 concentration was too high, the viscosity of the system increased dramatically (Fig. 3b), severely reducing the mass transfer efficiency and yield. Therefore, 60 wt% MaPa-4 was selected for the following study.

The ultrasonic extraction time was varied between 15 and 120 min (solid–liquid ratio: 40 mg mL^{-1} and MaPa-4 concentration: 60 wt%). With the increase of ultrasonic extraction time from 15 min to 60 min, the yield of HT was significantly increased from 2.07 mg g^{-1} to 4.35 mg g^{-1} (Fig. 3c) because the ultrasonic cavitation, mechanical and thermal effects accelerated the release, diffusion and dissolution of the effective substances into the solvent. However, the decrease in the HT yield with prolonged extraction time could be attributed to the decomposition of phenolic compounds under instantaneous temperature and pressure changes.

HT yields were measured when solid–liquid ratios were decreased from 200 to 10 mg mL^{-1} (MaPa-4 concentration: 60 wt% and extraction time: 60 min). A significant increase in the HT yield was observed when the solid–liquid ratio was varied between 200 and 20 mg mL^{-1} (Fig. 3d). However, after 20 mg mL^{-1}, HT did not increase significantly and even decreased slightly. As the solid–liquid ratio decreased, the enlarged contact area between the solvent and sample was favorable for extraction. However, when the solid–liquid ratio was below 20 mg mL^{-1}, the positive contribution of the enlarged contact area reached a threshold and the extraction was saturated. With further increase of the solvent ratio, the other dissolved components might cause the decomposition of HT. In summary, the maximum HT yield was 4.98 mg g^{-1} under the optimal extraction conditions, *i.e.*, 60 wt% of MaPa-4, 60 min extraction time, and 20 mg mL^{-1} solid–liquid ratio.

The extract obtained under the optimal conditions is denoted as MaPa-4 extract. Then, water was selected as the control solvent to extract HT. The yield was 3.34 mg g^{-1} under the conditions of 60 min extraction time and 20 mg mL^{-1} solid–liquid ratio, and the product is denoted as water extract.

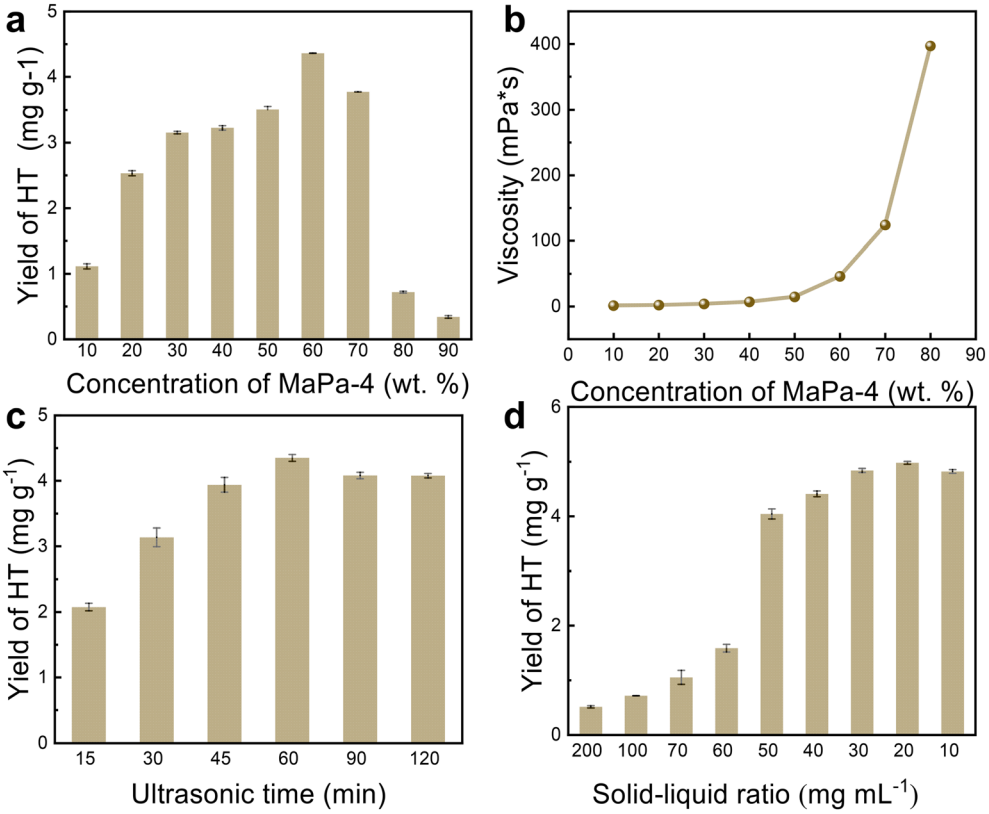

Fig. 3 Influence of different factors on the experiment. (a) Effect of the MaPa-4 concentration on the HT yield; (b) viscosity of MaPa-4 at different concentrations; (c) effect of the extraction time on the HT yield; (d) effect of the solvent/solid ratio on the HT yield.

2.4 Biocompatibility evaluation of the MaPa-4 extract

Human keratinocytes, human skin fibroblasts, and RAW 264.7 mouse macrophages were used as cell models to test the cytotoxicity of the MaPa-4 extract (Fig. 4b). For human keratinocytes, the relative survival rate was above 90% when the concentration of MaPa-4 extract was below 0.625 mg mL^{-1}, and its IC_{50} was 13.39 mg mL^{-1}. The relative survival rate of human skin fibroblasts was similar to that of human keratinocytes, and the IC_{50} was slightly lower (10.28 mg

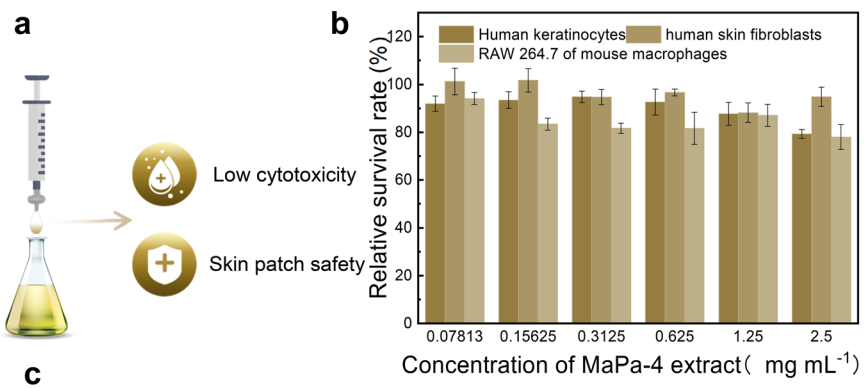

c

Group	Number of subjects	Observation time	Patch test number of different skin reaction levels				
			0	1	2	3	4
MaPa-4 extract	33	0.5 h	33	0	0	0	0
		24 h	33	0	0	0	0
		48 h	33	0	0	0	0
Negative control Blank + filter	33	0.5 h	33	0	0	0	0
		24 h	33	0	0	0	0
		48 h	33	0	0	0	0
The results of human skin patch test showed that 0 cases of 33 people had skin adverse reactions.							

Fig. 4 Biocompatibility evaluation of the MaPa-4 extract. (a) Schematic of the cytotoxicity and human skin spot tests; (b) cytotoxicity results of the MaPa-4 extract; (c) results of the human skin spot test.

mL^{-1}). For RAW 264.7 mouse macrophages, the relative survival rate was above 90% when the concentration of MaPa-4 extract was below 0.078125 mg mL^{-1}, and its IC_{50} was even lower (8.745 mg mL^{-1}). The human skin spot test of the MaPa-4 extract showed that none of 33 people had adverse skin reactions, suggesting its good biocompatibility.

2.5 Anti-inflammatory effect of the MaPa-4 extract

According to the relative survival rate of human keratinocytes, the anti-inflammatory effect of the MaPa-4 extract was tested within the cell safety concentration (<0.625 mg mL^{-1}). Different concentrations of MaPa-4 extract (0.1 mg mL^{-1}, 0.25 mg mL^{-1} and 0.5 mg mL^{-1}) were prepared for the experiment. As shown in Fig. 5b, no significant change was observed in the relative content of IL-1α when the concentrations of MaPa-4 extract were 0.25 mg mL^{-1} and 0.5 mg mL^{-1} ($P > 0.05$). At the concentration of 0.1 mg mL^{-1}, the relative content of IL-1α decreased significantly by 31.60% ($P < 0.05$), indicating that the MaPa-4 extract had a certain soothing effect at this concentration. Compared with the model control group, the relative contents of IL-8 in the MaPa-4 extract significantly decreased by 43.18%, 34.39% and 13.27% at the concentrations of 0.1 mg mL^{-1}, 0.25 mg mL^{-1} and 0.5 mg mL^{-1}, respectively ($P < 0.05$). This indicated that the MaPa-4 extract had a soothing effect at all tested concentrations. Compared with the model control group, the relative content of PGE2 in the MaPa-4 extract was significantly increased at 0.1 mg mL^{-1} ($P < 0.05$), but decreased by 55.81% and 33.56% at 0.5 mg mL^{-1} and 0.25 mg mL^{-1}, respectively ($P < 0.05$), indicating that the soothing effect only occurred at 0.5 mg mL^{-1} and 0.25 mg mL^{-1}.

In conclusion, the MaPa-4 extract inhibited IL-8 and PGE2 at 0.5 mg mL^{-1} and 0.25 mg mL^{-1} ($P < 0.05$). At the concentration of 0.1 mg mL^{-1}, it showed an inhibitory effect on IL-8 and IL-1α ($P < 0.05$).

2.6 Comparison of the anti-bacterial effects of the MaPa-4 extract and water extract

The anti-bacterial effects of the MaPa-4 extract and water extract were compared in this study. As shown in Fig. 6b, the diameters of the anti-bacterial ring of the negative control and water extract were both 6 mm, indicating that the water extract had no anti-bacterial effect on *Escherichia coli*. In contrast, the diameter of the anti-bacterial ring of the MaPa-4 extract was 13.93 mm, confirming the anti-bacterial effect of the MaPa-4 extract on *Escherichia coli*. This should be due to the intrinsic anti-bacterial properties of matrine.

2.7 Comparison of the antioxidant effects of the MaPa-4 extract and water extract

The extracts obtained by the two solvents under the same extraction conditions were used for the antioxidant test. The

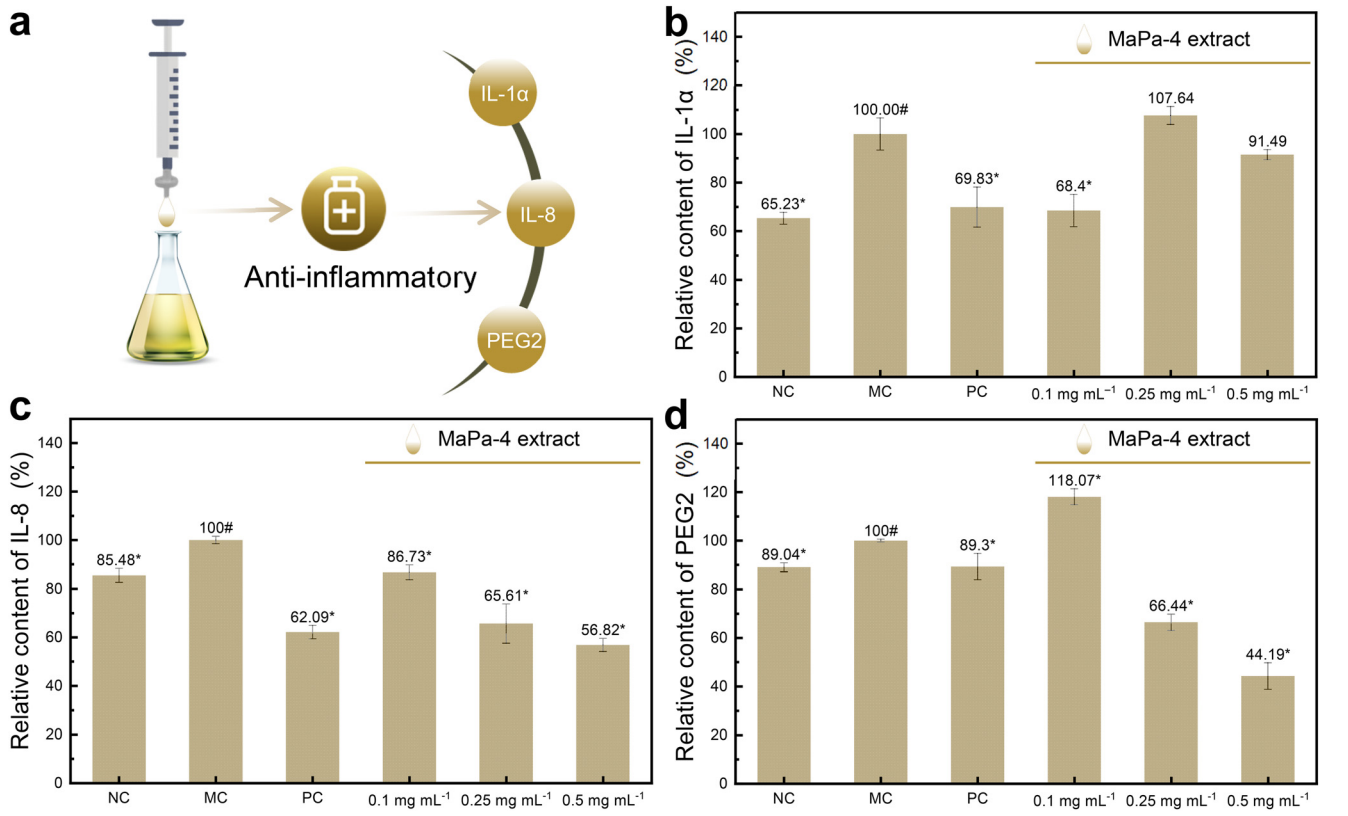

Fig. 5 Anti-inflammatory effect of the MaPa-4 extract. (a) Schematic of the anti-inflammatory test; (b) relative content of IL-1α; (c) relative content of IL-8; (d) relative content of PEG2 (for the negative control group, $^{\#}P < 0.05$ and for the model control group, $^{*}P < 0.05$).

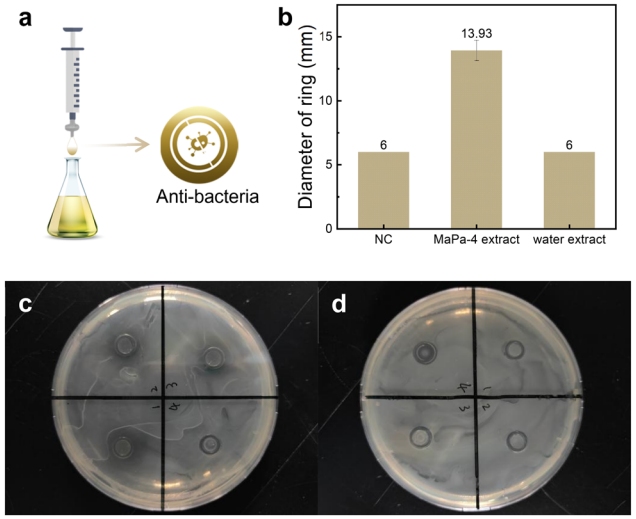

Fig. 6 Anti-bacterial effects of MaPa-4 and water extracts. (a) Schematic of the anti-bacterial test; (b) diameter of the anti-bacterial ring; (c) image of the anti-bacterial experiment using the MaPa-4 extract; (d) image of the anti-bacterial experiment using the water extract.

DPPH free radical scavenging curves of the MaPa-4 extract and water extract are shown in Fig. 7b and c, respectively. The IC_{50} values of the MaPa-4 and water extracts were 69% and 13.29%, respectively. The MaPa-4 extract had stronger scavenging ability for DPPH free radicals than the water extract. The $ABTS^+$ free radical scavenging curves of the MaPa-4 extract and water extract are shown in Fig. 7d and e, respectively. The IC_{50} value of the MaPa-4 extract was 0.88% and the IC_{50} value of the water extract was 1.74%. The MaPa-4 extract showed a better scavenging effect on $ABTS^+$ free radicals than the water extract. When the reduction rate of 0.2 mg mL^{-1} VC to ferrous ions was 100%, the relative reduction rate curves of the MaPa-4 extract and water extract are shown in Fig. 7f and g, respectively. The IC_{50} value of the MaPa-4 extract was 4.24% and the IC_{50} value of the water extract was 7.18%. The reduction effect of the MaPa-4 extract on ferrous ions was better than that of the water extract. The scavenging results of the MaPa-4 extract and water extract on $^{\cdot}OH$ free radicals are shown in Fig. 7h. At a low concentration, neither of them could capture $^{\cdot}OH$ free radicals. When the concentration was increased to 40%, both extracts showed a similar clearance effect without significant difference. The scavenging results of the MaPa-4 extract and water extract on $^{\cdot}O_2$-free radicals are shown in Fig. 7i. Both extracts had no scavenging effect on $^{\cdot}O_2$-free radicals at various concentrations.

Based on the above results, the MaPa-4 extract contained a higher concentration of HT and also showed better free radical scavenging and reducing ability than the water extract. It can be further developed as an antioxidant.

3 Conclusion

An ultrasonic-assisted DES was developed for efficient and environmentally friendly extraction of HT from olive leaves. MaPa-4 was used as the best solvent for single factor experiments. A maximum HT yield of 4.98 mg g^{-1} was achieved under the optimal extraction conditions, *i.e.*, 60 wt% of MaPa-4, 60 min extraction time, and 20 mg mL^{-1} solid–liquid ratio. The formation mechanism of MaPa and its interaction with HT were analyzed by FTIR, NMR and DFT calculation. MaPa-4 and water extracts obtained under the same extraction conditions were used for a series of efficacy tests. The results showed that the MaPa-4 extract had low cytotoxicity and excellent biocompatibility. In addition, the MaPa-4 extract showed anti-inflammatory and bacteriostatic effects at certain concentrations. The antioxidant effects of MaPa-4 were superior to those of the water extract in terms of DPPH and $ABTS^+$ clearance and total reducing capacity. Therefore, this study successfully explored an ultrasonic assisted natural deep eutectic solvent for extracting HT from olive leaves, and a series of efficacy studies based on the extract solution shed light on the development of related products of the olive leaf extract.

4 Experimental materials and methods

4.1 Materials

The HT standard (purity >98%) was purchased from Shanghai Aladdin Biochemical Technology Co., Ltd. Olive leaf raw materials were purchased from Sichuan Hua'ou Olive Development Co., Ltd. Matrine (purity >98%) was purchased from Jiangsu Tiansheng Pharmaceutical Co., Ltd. Panthenol (purity >98%) was purchased from Guangzhou Hengtao Trading Co., Ltd. Olive leaves were crushed and sifted through a 60-mesh screen. Then, the powder was stored in a freezer for further experiments. The ball-and-stick models of matrine and panthenol are shown in Fig. 8. All chemicals are used as received without further treatment.

4.2 Preparation and characterization of DESs

Matrine and panthenol with different molar ratios were put into a reactor and heated at 50 °C for 8 h with stirring, and the resulting light-yellow viscous liquid was denoted as matrine–panthenol DES (MaPa). A certain amount of ultrapure water was added to the light-yellow viscous liquid to obtain a clear, transparent, and uniform MaPa solution (30 wt%). The composition and physicochemical properties of the prepared DESs are listed in Table 1. The electrical conductivity was tested using a Lei Ci multi-parameter analyzer and the viscosity was tested using an SV-A/SV-H series viscometer. The chemical structure of MaPa and its monomers was analyzed by ^1H NMR (Avance III 400 MHz purchased from Bruker in Germany) and FTIR (Nicolet iS 50 purchased from Thermo Fisher in America). TGA was performed in N_2 with a heating rate of 10 °C min^{-1} on a thermal analyzer (Mettler TGA2 purchased from Mettler Toledo Technology Co., Ltd. in China). DSC curves were measured with N_2 as a purifying gas and the system was cooled with liquid N_2 on a thermal analyzer (Mettler DSC3

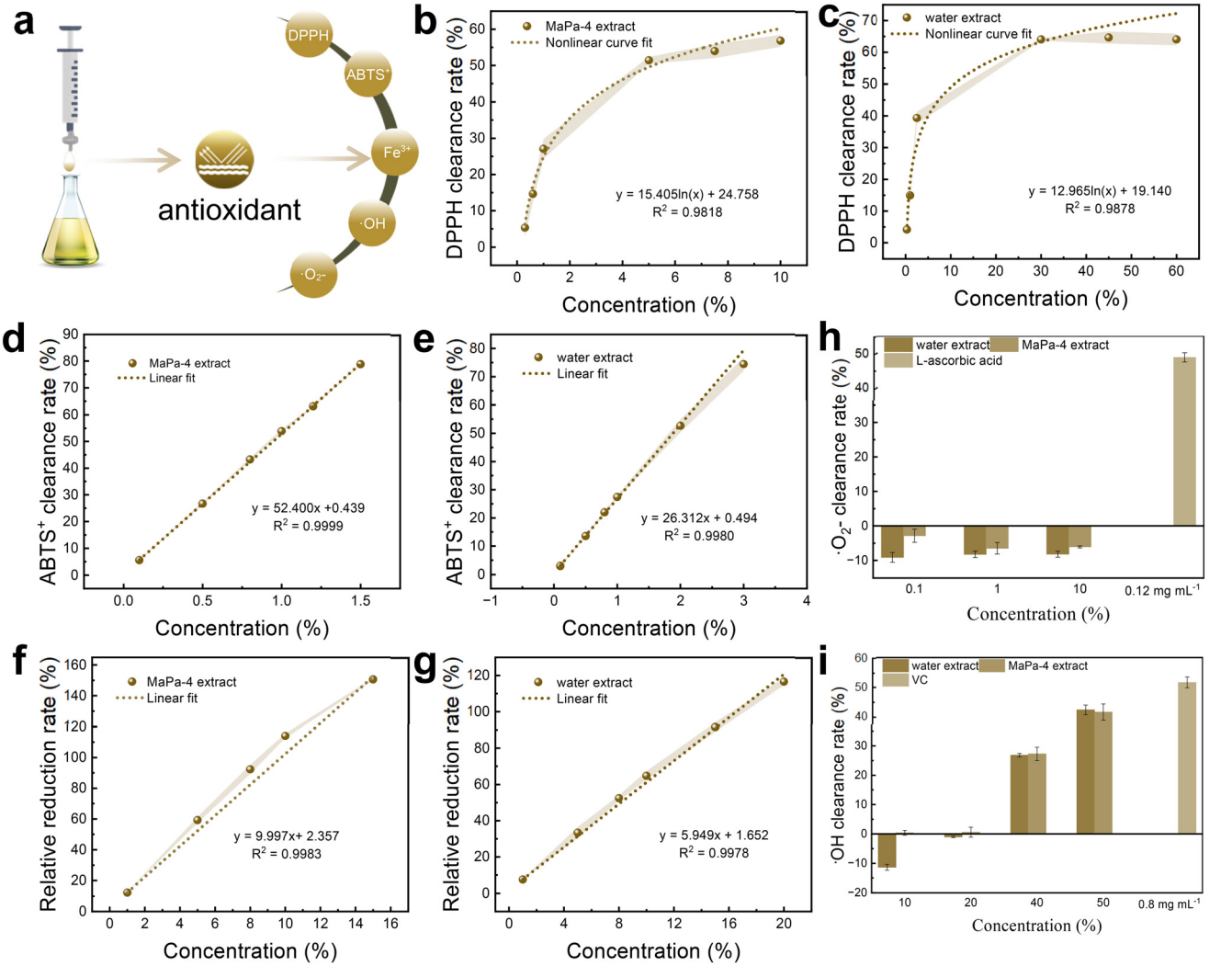

Fig. 7 Antioxidant effects of MaPa-4 and water extracts. (a) Schematic of the antioxidant test; DPPH free radical scavenging curves of (b) MaPa-4 and (c) water extracts; $ABTS^+$ free radical scavenging curves of (d) MaPa-4 and (e) water extracts; relative reduction rate curves of (f) MaPa-4 and (g) water extracts; scavenging results of MaPa-4 and water extracts on (h) $^{\cdot}OH$ free radicals and (i) $^{\cdot}O_2$ free radicals.

purchased from Mettler Toledo Technology Co., Ltd. in Switzerland) at a rate of 10 °C min^{-1}. Gaussian 16 software[38] was used to optimize the molecular structure and calculate the frequency and surface electrostatic potential at the theoretical level of B3LYP-D3(BJ)/6-311G**. IRI[39] was used in Multiwfn[40] to analyze the weak interaction in the system, and visualization operation was carried out in combination with the VMD program.[41]

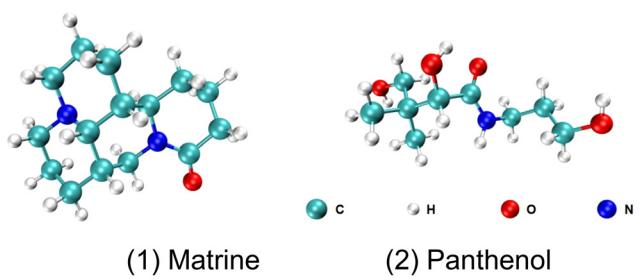

Fig. 8 Ball-and-stick models of matrine and panthenol.

4.3 Ultrasound assisted extraction of HT

Olive leaf powder was added to water, methanol, ethanol or 30 wt% MaPa at a concentration of 40 mg mL^{-1} and subjected to ultrasonic extraction experiments in an ultrasonic cleaning machine (XM-P102H, 300 W) at 30 °C for 60 min. The plant extract was centrifuged at 10 000 rpm for 15 min and the supernatant was diluted ten times, and then filtered through a 0.45 μm PTFE membrane syringe filter (VWR).

4.4 Chromatographic quantification (HPLC) analysis

A C18 column (IntersilSustain, 5 μm) was used in HPLC-UV (Agilent 1100) to determine the concentration of HT. The mobile phase consists of methanol (0.1% formic acid) (eluent

Table 1 Composition and physicochemical properties of the prepared DESs

DES	HBA	HBD	Molar ratio	Conductivity of 30 wt% DESs (ms cm^{-1})	Viscosity of 30 wt% DESs (mPa*s)
MaPa-1	Matrine	Panthenol	1 : 1	206	3.90
MaPa-2	Matrine	Panthenol	1 : 2	270	3.55
MaPa-3	Matrine	Panthenol	1 : 3	337	3.53
MaPa-4	Matrine	Panthenol	1 : 4	363	3.31

A) and water (0.1% formic acid) (eluent B). The column temperature was set at 30 °C, and the gradient elution sequence was from 0 min (5% eluent A and 95% eluent B) to 26 min (95% eluent A and 5% eluent B). The injection volume was 10 μL and the flow rate was 1.0 mL min^{-1}. The absorbance of the eluent was measured at 280 nm, and the retention time was 8.32 min. The concentration of HT was calculated by the linear least squares method. All calculations are reported as per gram of olive leaf.

4.5 Microstructure analysis of olive leaf powder

FE-SEM (Hitachi SU8018) was used to observe the microstructure of olive leaf powder before and after treatment in a SE mode. Prior to testing, the sample was sprayed with gold to facilitate electrical conduction.

4.6 Single factor experiment

To explore the best extraction conditions, the main factors affecting the yield of HT, *i.e.*, the DES concentration (10–90 wt%), ultrasonic time (15–120 min), and solid–liquid ratio (200–10 mg mL^{-1}) were explored. When performing a single-factor test, one parameter was varied when the other two parameters were fixed, as shown in Table 2.

Based on the above single factor experiment, there will be corresponding optimal extraction conditions. Under these conditions, extracts based on MaPa-4 and ultrapure water were used in a series of analytical tests, denoted as MaPa-4 extract and water extract.

4.7 Biocompatibility test of the MaPa-4 extract

The colorimetric MTT assay was used to evaluate the cytotoxic effects of DES extracts.[42] The suspensions of human keratinocytes (purchased from Procell Life Science&Technology Co., Ltd.), human skin fibroblasts (purchased from Guangdong Biocell Biotechnology Co., Ltd.) and RAW 264.7 mouse macrophages (purchased from Chinese Academy of Medical Sciences) (100 μL) were inoculated into a 96-well plate and incubated for 24 h for cell adherence. The medium was discarded and 100 μL of the sample solution was replaced. After incubating the cells for 24 h, 10 μL of MTT solution was added, and the plate was placed in an incubator for 4 h. The culture medium was then discarded, followed by adding 150 μL of DMSO and shaking for 10 min. The optical density at 490 nm (OD 490 nm) was measured and the relative survival rate was calculated using eqn (1).

$$\text{Relative survival rate } \% = \frac{\text{TestOD}_{490\ \text{nm}}}{\text{NegOD}_{490\ \text{nm}}} \times 100\% \quad (1)$$

where $\text{TestOD}_{490\ \text{nm}}$ and $\text{NegOD}_{490\ \text{nm}}$ are the mean $\text{OD}_{490\ \text{nm}}$ values of the tested substance and negative control, respectively.

Table 2 Single factor experimental conditions

DES concentration (wt%)	10	20	30	40	50	60	70	80	90
Ultrasonic time (min)	15	30	45	60	90	120			
Solid–liquid ratio (mg mL^{-1})	200	100	70	60	50	40	30	20	10

4.8 Human skin patch experiment of the MaPa-4 extract

According to Chapter VII in the Technical Specifications for Cosmetic Safety (2015 edition), the potential adverse reactions of cosmetic products to the human skin were tested. A qualified patch test device was selected, and 0.020–0.025 mL of the tested substance was placed in the patch test device. The device was externally affixed with hypoallergenic tape to the curved side of the subject's forearm. The device was removed 24 h later, and the skin reaction was observed at 0.5, 24 and 48 h after removal. The results were recorded according to the skin reaction grading standard in the Technical Specifications for Cosmetic Safety (2015 edition).

4.9 Anti-inflammatory efficacy test of the MaPa-4 extract

By using human keratinocytes induced by LPS as an *in vitro* inflammatory cell model, inflammatory factors (IL-1α, IL-8, PGE2) secreted in the supernatant were detected using an ELISA kit to evaluate the anti-inflammatory efficacy. In detail, human keratinocyte suspension was inoculated into a 12-well plate and cultured in an incubator.

Working liquids, including negative, model and positive control groups and sample groups, were prepared according to the test plan (Table 3). The negative control group only contained MEM culture medium, and the model control group included MEM culture medium and LPS. The MEM culture medium contains 4.5 g L^{-1} D-glucose, 10% fetal bovine serum, and 1% mixed antibiotics. The MEM culture solution with different concentrations of test samples was added to each well of the sample group. In the positive control group, LPS and dexamethasone-containing MEM culture medium were added. Each group was duplicated in 3 different wells, and the culture was conducted for 24 ± 1 h. The contents of IL-1α, IL-8 and PGE2 in the supernatant were determined using an ELISA kit.

Table 3 Anti-inflammatory efficacy test scheme

	Sample information		Detection method			
Experimental group	Name	Concentration	Induction conditions	Detection model	Detection index	Detection means
Negative control group (NC)	—	—	—	Human keratinocytes	IL-1α, IL-8, PGE2	ELISA
Model control group (MC)	—	—	LPS			
Positive control group (PC)	Dexamethasone	—				
Sample set	MaPa-4 extract	0.1 mg mL^{-1} 0.25 mg mL^{-1} 0.5 mg mL^{-1}				

4.10 Comparison of the bacteriostatic effects of the MaPa-4 extract and water extract

According to QB/T 2738-2012 "Evaluation Method for Anti-bacterial and Bacteriostatic Effect of Daily Chemical Products", the bacteriostatic ability against *Escherichia coli* (purchased from Guangdong Institute of Microbiology) was tested by continuously dissolving the bacteriostatic agent through agar diffusion to form different concentration gradients. The diameter of the inhibition ring was used to determine the anti-bacterial ability. A diameter larger than 7 mm is considered an excellent bactericide.

4.11 Comparison of the antioxidant activity of the MaPa-4 extract and water extract

MaPa-4 and water extracts were tested for antioxidant properties, including DPPH, $ABTS^+$ and total reducing power. The sample concentration is expressed by volume percentage. The experimental procedures are based on T/SHRH 006-2018 "Cosmetics – Free Radical (DPPH) Scavenging Experimental Method", XJJC-SOP3-12-001/2021 "Cosmetics – Free Radical ($ABTS^+$) Scavenging Experimental Method", XJJC-SOP3-16-001/2021 "Cosmetics – Determination of Reducing Power", XJJC-SOP3-13-001/2021 "Cosmetics – Free Radical ($^{\cdot}OH$) Scavenging Experimental Method", and XJJC-SOP3-11-001/2021 "Cosmetics – Free Radical ($^{\cdot}O_2^-$) Scavenging Experimental Method".

Abbreviations

DES	Deep eutectic solvent
NADES	Natural deep eutectic solvent
HPLC	High performance liquid chromatography
FE-SEM	Field emission scanning electron microscopy
SE	Secondary electron
HT	Hydroxytyrosol
DFT	Density functional theory
TGA	Thermogravimetric analysis
DSC	Differential scanning calorimetry
IRI	Interaction region indicator function
ESP	Electrostatic potential analysis
FTIR	Fourier transform infrared spectroscopy
^{1}H NMR	Nuclear magnetic resonance hydrogen spectrum

Data availability

All the relevant data are available from the corresponding authors upon reasonable request.

Author contributions

Mingming Hu: investigation, methodology, writing – original draft, supervision, validation, formal analysis, project administration. Bao Han: conceptualization, original draft revision, supervision, validation, formal analysis. Lin Xie: writing – review & editing. Beibei Lu: writing – review & editing. De Bai: writing – review & editing. Nuo Shi: writing – review & editing. Ya Liao: review & editing. Yan Wang: review & editing. Ling Liu: review & editing. Shaojun Wu: review & editing. Runrui Lan: review & editing. Xiaomei Lei: review & editing. Ci Shi: review & editing. Danhua Huang: review & editing. Yuanbin Li: supervision. Lin Lin: funding acquisition, project administration, supervision. Jiaheng Zhang: funding acquisition, project administration, resources, supervision.

Conflicts of interest

The authors declare no conflict of interest.

Acknowledgements

This work was financially supported by the National Natural Science Foundation of China (21905069, U21A20307), the Shenzhen Science and Technology Innovation Committee (Grant No. ZDSYS20190902093220279, KQTD20170809110344233, GXWD20201230155427003-20200821181245001,GXWD20201230155427003-20200821181809001, ZX20200151), and the Department of Science and Technology of Guangdong Province (Grant No. 2020A1515110879).

References

1 M. Ansari, M. Kazemipour and S. Fathi, Development of a simple green extraction procedure and HPLC method for determination of oleuropein in olive leaf extract applied to a multi-source comparative study, *J. Iran. Chem. Soc.*, 2011, **8**, 38–47.

2 G. Bartolini, G. Prevost, C. Messeri and G. Carignani, *Olive germplasm: Cultivars and world-wide collections*, FAO Library, Rome, 1998.
3 J. J. Yuan, C. Z. Wang, J. Z. Ye, R. Tao and Y. S. Zhang, Enzymatic hydrolysis of oleuropein from olea europea (olive) leaf extract and antioxidant activities, *Molecules*, 2015, **20**, 2903–2921.
4 B. Letutour and D. Guedon, Antioxidative activities of olea-europaea leaves and related phenolic-compounds, *Phytochemistry*, 1992, **31**, 1173–1178.
5 O. H. Lee, B. Y. Lee, J. Lee, H. B. Lee, J. Y. Son, C. S. Park, K. Shetty and Y. C. Kim, Assessment of phenolics-enriched extract and fractions of olive leaves and their antioxidant activities, *Bioresour. Technol.*, 2009, **100**, 6107–6113.
6 S. Şahin, M. Bilgin and M. U. Dramur, Investigation of oleuropein content in olive leaf extract obtained by supercritical fluid extraction and Soxhlet methods, *Sep. Sci. Technol.*, 2011, **46**, 1829–1837.
7 I. Fki, N. Allouche and S. Sayadi, The use of polyphenolic extract, purified hydroxytyrosol and 3,4-dihydroxyphenyl acetic acid from olive mill wastewater for the stabilization of refined oils: A potential alternative to synthetic antioxidants, *Food Chem.*, 2005, **93**, 197–204.
8 L. Martinez, G. Ros and G. Nieto, Hydroxytyrosol: Health benefits and use as functional ingredient in meat, *Medicines*, 2018, **5**, 13.
9 A. Voltes, A. Bermúdez, G. Rodríguez-Gutiérrez, M. L. Reyes, C. Olano, J. Fernández-Bolaños and F. de la Portilla, Anti-inflammatory local effect of hydroxytyrosol combined with pectin-alginate and olive oil on trinitrobenzene sulfonic acid-induced colitis in wistar rats, *J. Invest. Surg.*, 2020, **33**, 8–14.
10 R. Crea, C. M. Bitler, L. M. Bolin and P. Pontoniere, Anti-inflammatory activity of hydroxytyrosol inhibition of cytokine production in a parkinson's model system of neuroinflammation, *Agro Food Ind. Hi-Tech*, 2012, **23**, 26–29.
11 A. Smeriglio, M. Denaro, L. Mastracci, F. Grillo, L. Cornara, S. Shirooie, S. M. Nabavi and D. Trombetta, Safety and efficacy of hydroxytyrosol-based formulation on skin inflammation: in vitro evaluation on reconstructed human epidermis model, Daru, *J. Pharm. Sci.*, 2019, **27**, 283–293.
12 C. G. Guex, F. Z. Reginato, P. R. de Jesus, J. C. Brondani, G. H. H. Lopes and L. D. F. Bauermann, Antidiabetic effects of Olea europaea L. leaves in diabetic rats induced by high-fat diet and low-dose streptozotocin, *J. Ethnopharmacol.*, 2019, **235**, 1–7.
13 F. Vlavcheski, M. Young and E. Tsiani, Antidiabetic effects of hydroxytyrosol: In vitro and in vivo evidence, *Antioxidants*, 2019, **8**, 6.
14 K. Shimazu, S. Fukumitsu, T. Ishijima, T. Toyoda, Y. Nakai, K. Abe, K. Aida, S. Okada and A. Hino, The anti-arthritis effect of olive-derived maslinic acid in mice is due to its promotion of tissue formation and its anti-inflammatory effects, *Mol. Nutr. Food Res.*, 2019, **63**, 1800543.
15 A. Mahmoudi, F. Hadrich, I. Feki, H. Ghorbel, Z. Bouallagui, R. Marrekchi, H. Fourati and S. Sayadi, Oleuropein and hydroxytyrosol rich extracts from olive leaves attenuate liver injury and lipid metabolism disturbance in bisphenol a-treated rats, *Food Funct.*, 2018, **9**, 3220–3234.
16 Y. Yonezawa, T. Miyashita, H. Nejishima, Y. Takeda, K. Imai and H. Ogawa, Anti-inflammatory effects of olive-derived hydroxytyrosol on lipopolysaccharide-induced inflammation in RAW264.7 cells, *J. Vet. Med. Sci.*, 2018, **80**, 1801–1807.
17 Z. Bouallagui, M. Bouaziz, S. Lassoued, J. M. Engasser, M. Ghoul and S. Sayadi, Hydroxytyrosol acyl esters: Biosynthesis and activities, *Appl. Biochem. Biotechnol.*, 2011, **163**, 592–599.
18 A. Khoddami, M. A. Wilkes and T. H. Roberts, Techniques for analysis of plant phenolic compounds, *Molecules*, 2013, **18**, 2328–2375.
19 M. Roy, S. Chakrabarty, D. Sinha, R. K. Bhattacharya and M. Siddiqi, Anticlastogenic, antigenotoxic and apoptotic activity of epigallocatechin gallate: A green tea polyphenol, *Mutat. Res., Fundam. Mol. Mech. Mutagen.*, 2003, **523-524**, 33–41.
20 R. Wang, F. Pan, R. He, F. Kuang, L. Wang and X. Lin, Arecanut (Areca catechu L.) seed extracts extracted by conventional and eco-friendly solvents: Relation between phytochemical compositions and biological activities by multivariate analysis, *J. Appl. Res. Med. Aromat. Plants*, 2021, **25**, 100336.
21 F. Chemat, M. A. Vian and G. Cravotto, Green extraction of natural products: Concept and principles, *Int. J. Mol. Sci.*, 2012, **13**, 8615–8627.
22 F. Chemat, M. Abert-Vian, A. S. Fabiano-Tixier, J. Strube, L. Uhlenbrock, V. Gunjevic and G. Cravotto, Green extraction of natural products. Origins, current status, and future challenges, *TrAC, Trends Anal. Chem.*, 2019, **118**, 248–263.
23 A. P. Abbott, G. Capper, D. L. Davies, R. K. Rasheed and V. Tambyrajah, Novel solvent properties of choline chloride/urea mixtures, *Chem. Commun.*, 2003, 70–71.
24 X. Fu, D. Wang, T. Belwal, Y. Xu, L. Li and Z. Luo, Sonication-synergistic natural deep eutectic solvent as a green and efficient approach for extraction of phenolic compounds from peels of carya cathayensis sarg, *Food Chem.*, 2021, **355**, 129577.
25 B. M. Popovic, N. Micic, A. Potkonjak, B. Blagojevic, K. Pavlovic, D. Milanov and T. Juric, Novel extraction of polyphenols from sour cherry pomace using natural deep eutectic solvents-ultrafast microwave-assisted NADES preparation and extraction, *Food Chem.*, 2022, **366**, 130562.
26 Y. Liu, W. Zhe, R. Zhang, Z. Peng, Y. Wang, H. Gao, Z. Guo and J. Xiao, Ultrasonic-assisted extraction of polyphenolic compounds from Paederia scandens (Lour.) Merr. Using deep eutectic solvent: Optimization, identification, and comparison with traditional methods, *Ultrason. Sonochem.*, 2022, **86**, 106005.
27 M. Nemati, M. Tuzen, N. Altunay, M. A. Farajzdeh, F. Abdi and M. R. Afshar Mogaddam, Development of sodium hydroxide-induced homogenous liquid-liquid extraction-effervescent assisted dispersive liquid-liquid microextraction based on deep eutectic solvents; Application in the extraction of phytosterols from cow cream samples, *J. Food Compos. Anal.*, 2022, **106**, 104291.

28 M. Nemati, M. R. A. Mogaddam, M. A. Farazajdeh, M. Tuzen and J. Khandaghi, In-situ formation/decomposition of deep eutectic solvent during solidification of floating organic droplet-liquid-liquid microextraction method for the extraction of some antibiotics from honey prior to high performance liquid chromatography-tandem mass spectrometry, *J. Chromatogr. A*, 2021, **1660**, 462653.
29 O. A. Olalere and C.-Y. Gan, Process optimisation of defatted wheat germ protein extraction in a novel alkaline-based deep eutectic solvent (DES) via Box–Behnken experimental design (BBD), *Food Chem.*, 2023, **409**, 135224.
30 X. Chen, R. Wang and Z. Tan, Extraction and purification of grape seed polysaccharides using pH-switchable deep eutectic solvents-based three-phase partitioning, *Food Chem.*, 2023, **412**, 135557.
31 Q. Yu, F. Wang, Y. Jian, V. M. Chernyshev, Y. Zhang, Z. Wang, Z. Yuan and X. Chen, Extraction of flavonoids from Glycyrrhiza residues using deep eutectic solvents and its molecular mechanism, *J. Mol. Liq.*, 2022, **363**, 119848.
32 J. Lei, Y. Wang, W. Li, S. Fu, J. Zhou, D. Lu, C. Wang, X. Sheng, M. Zhang, S. Xiao, C. Sun and G. Wang, Natural green deep eutectic solvents-based eco-friendly and efficient extraction of flavonoids from Selaginella moellendorffii: Process optimization, composition identification and biological activity, *Sep. Purif. Technol.*, 2022, **283**, 120203.
33 H. Wu, C. Liu, Y. Yang, J. Xue, Z. Ke, W. Zheng, T. Li, Y. Sun and C. Zhang, Preliminary exploration of the mechanism of compound Qinlan oral liquid against new coronavirus pneumonia based on network pharmacology and molecular docking technology, *TMR Mod. Herb. Med.*, 2020, **3**, 128–177.
34 Y.-H. Hsieh, Y. Li, Z. Pan, Z. Chen, J. Lu, J. Yuan, Z. Zhu and J. Zhang, Ultrasonication-assisted synthesis of alcohol-based deep eutectic solvents for extraction of active compounds from ginger, *Ultrason. Sonochem.*, 2020, **63**, 104915.
35 Z. Pan, Y. Bo, Y. Liang, B. Lu, J. Zhan, J. Zhang and J. Zhang, Intermolecular interactions in natural deep eutectic solvents and their effects on the ultrasound-assisted extraction of artemisinin from Artemisia annua, *J. Mol. Liq.*, 2021, **326**, 115283.
36 H. Zhang, L. Chen, X. Sun, Q. Yang, L. Wan and C. Guo, Matrine: A promising natural product with various pharmacological activities, *Front. Pharmacol.*, 2020, **11**, 588.
37 F. B. Camargo Jr., L. R. Gaspar and P. M. B. G. Maia Campos, Skin moisturizing effects of panthenol-based formulations, *J. Cosmet. Sci.*, 2011, **62**, 361–369.
38 M. J. Frisch, G. W. Trucks, H. B. Schlegel, G. E. Scuseria, M. A. Robb, J. R. Cheeseman, G. Scalmani, V. Barone, G. A. Petersson, H. Nakatsuji, X. Li, M. Caricato, A. V. Marenich, J. Bloino, B. G. Janesko, R. Gomperts, B. Mennucci, H. P. Hratchian, J. V. Ortiz, A. F. Izmaylov, J. L. Sonnenberg, D. Williams-Young, F. Ding, F. Lipparini, F. Egidi, J. Goings, B. Peng, A. Petrone, T. Henderson, D. Ranasinghe, V. G. Zakrzewski, J. Gao, N. Rega, G. Zheng, W. Liang, M. Hada, M. Ehara, K. Toyota, R. Fukuda, J. Hasegawa, M. Ishida, T. Nakajima, Y. Honda, O. Kitao, H. Nakai, T. Vreven, K. Throssell, J. A. Montgomery Jr., J. E. Peralta, F. Ogliaro, M. J. Bearpark, J. J. Heyd, E. N. Brothers, K. N. Kudin, V. N. Staroverov, T. A. Keith, R. Kobayashi, J. Normand, K. Raghavachari, A. P. Rendell, J. C. Burant, S. S. Iyengar, J. Tomasi, M. Cossi, J. M. Millam, M. Klene, C. Adamo, R. Cammi, J. W. Ochterski, R. L. Martin, K. Morokuma, O. Farkas, J. B. Foresman and D. J. Fox, *Gaussian 16 Rev. C.01.*, 2016.
39 T. Lu and Q. Chen, Interaction region indicator: A simple real space function clearly revealing both chemical bonds and weak interactions, *Chem.: Methods*, 2021, **1**, 231–239.
40 T. Lu and F. W. Chen, Multiwfn: A multifunctional wavefunction analyzer, *J. Comput. Chem.*, 2012, **33**, 580–592.
41 W. Humphrey, A. Dalke and K. Schulten, VMD: Visual molecular dynamics, *J. Mol. Graphics*, 1996, **14**, 33–38.
42 I. P. E. Macário, H. Oliveira, A. C. Menezes, S. P. M. Ventura and F. J. M. Gonalves, Cytotoxicity profiling of deep eutectic solvents to human skin cells, *Sci. Rep.*, 2019, **9**, 3932.